

Applied comparisons between SCHA and R-SCHA regional modeling techniques

E. Thébault, L. Gaya-Piqué

▶ **To cite this version:**

E. Thébault, L. Gaya-Piqué. Applied comparisons between SCHA and R-SCHA regional modeling techniques. Geochemistry, Geophysics, Geosystems, 2008, 9, 10.1029/2008GC001953 . insu-03603719

HAL Id: insu-03603719
https://insu.hal.science/insu-03603719

Submitted on 10 Mar 2022

HAL is a multi-disciplinary open access archive for the deposit and dissemination of scientific research documents, whether they are published or not. The documents may come from teaching and research institutions in France or abroad, or from public or private research centers.

L'archive ouverte pluridisciplinaire **HAL**, est destinée au dépôt et à la diffusion de documents scientifiques de niveau recherche, publiés ou non, émanant des établissements d'enseignement et de recherche français ou étrangers, des laboratoires publics ou privés.

Copyright

Geochemistry Geophysics Geosystems G3
AN ELECTRONIC JOURNAL OF THE EARTH SCIENCES
Published by AGU and the Geochemical Society

Technical Brief
Volume 9, Number 7
3 July 2008
Q07005, doi:10.1029/2008GC001953
ISSN: 1525-2027

Applied comparisons between SCHA and R-SCHA regional modeling techniques

E. Thébault and L. Gaya-Piqué

Equipe de Géomagnétisme, Institut de Physique du Globe de Paris, Place Jussieu, F-75252 Paris CEDEX 5, France (ethebault@ipgp.jussieu.fr)

[1] Spherical cap harmonic analysis (SCHA) has become a common tool for the regional modeling of potential fields since its introduction by Haines (1985). The fact that SCHA satisfies Laplace equation and the possibility of representing high-frequency fields with a small number of coefficients (compared to the global spherical harmonic analysis) made SCHA the preferred choice for the development, for example, of magnetic field models at national scale. However, Thébault et al. (2006a) demonstrated that the traditional SCHA presented some deficiencies, in particular related to the inversion of multilevel data sets. The authors presented the R-SCHA technique as an alternative method in which the introduction of a new set of basis functions and boundary conditions solved this issue. In this paper we present some numerical comparisons between the SCHA and R-SCHA techniques applied with different synthetic vector data sets, from near-surface main field, main difference, and crustal field data simulating a World Digital Magnetic Anomaly Map subset. Other analyses are carried out with synthetic vector data set that mimics the expected data distribution from a multisatellite mission like the forthcoming European Swarm mission. No regularization, weighting, or ad hoc procedures are applied to the synthetic vector data, and a cap of 7° aperture is considered. The numerical analyses show that SCHA is a satisfying approximation in a band-limited spectral region that depends on the cap's size. It does not work correctly either for main field or for the short-scale crustal field modeling. These aspects are supported by equations illustrating why SCHA may fail. On the contrary, R-SCHA converges more slowly than SCHA but is valid in all cases. It gives a consistent set of regional coefficients and fits the radial variation of the field in a realistic way. At last, the special case of data incompatibility shows that R-SCHA does not fit incompatible data while SCHA assimilates most of them. These results should help the scientific community to evaluate the level of approximation needed for the development of regional magnetic field models in the era of the European Space Agency Swarm mission.

Components: 5732 words, 20 figures, 1 table.

Keywords: regional modeling; SCHA; R-SCHA.

Index Terms: 1517 Geomagnetism and Paleomagnetism: Magnetic anomalies: modeling and interpretation; 1541 Geomagnetism and Paleomagnetism: Satellite magnetics: main field, crustal field, external field.

Received 22 January 2008; **Revised** 7 April 2008; **Accepted** 9 May 2008; **Published** 3 July 2008.

Thébault, E., and L. Gaya-Piqué (2008), Applied comparisons between SCHA and R-SCHA regional modeling techniques, *Geochem. Geophys. Geosyst.*, *9*, Q07005, doi:10.1029/2008GC001953.

Copyright 2008 by the American Geophysical Union

1. Introduction

[2] Spherical cap harmonic analysis (SCHA [*Haines*, 1985]) has been the most used modeling technique for all kinds of geomagnetic studies at regional scales during the last two decades (see Table 1 of *Torta et al.* [2006] for a review). SCHA potential V_{SCHA} is a solution of the Laplace equation over a bounded regional cap of half-angle θ_0:

$$V_{SCHA} = a\sum_{k\geq m}\sum_{m\geq 0}\left(\frac{a}{r}\right)^{n_k+1} \cdot \left(g_{n_k}^{i,m}\cos(m\varphi) + h_{n_k}^{i,m}\sin(m\varphi)\right)P_{n_k}^{m}(\theta) + a\sum_{k\geq m}\sum_{m\geq 0}\left(\frac{r}{a}\right)^{n_k}\left(g_{n_k}^{e,m}\cos(m\varphi) + h_{n_k}^{e,m}\sin(m\varphi)\right) \cdot P_{n_k}^{m}(\theta) \quad (1)$$

with g_{nk}^{m} and h_{nk}^{m}, the SCHA coefficients defining the internal and external potentials, represented by the superscript i and e. The associated Legendre functions $P_{nk}^{m}(\theta)$ satisfy mixed boundary conditions on θ_0, giving rise to real degrees n_k, where k is an ordering index.

[3] Despite the apparently realistic results offered by the technique and its popularization through the publication of a software package [*Haines*, 1988], there are limitations that have been brought to light by applying the technique. These deficiencies (discussed in section 2) can all be explained by the incompleteness of the basis functions.

[4] A variety of solutions under the homonymous name revised spherical cap harmonic analysis (R-SCHA) were presented to solve most of the SCHA drawbacks. The early version proposed by *Thébault et al.* [2004] requires a flux correction to be fully efficient. Another development [*Thébault et al.*, 2006a] is directly suitable for inverse problems involving multilevel data sets [*Thébault et al.*, 2006b]. For the case of data available only at one surface, R-SCHA2D has been recently proposed and should provide the best model coefficients [*Thébault*, 2008].

[5] These different solutions behave diversely depending on the chosen boundary conditions, the amount of data and their distribution: if the flux-corrected solution given by *Thébault et al.* [2004] is particularly efficient for representing the main magnetic field, the solution given by *Thébault et al.* [2006a] is more convenient when dealing with the lithospheric field, and R-SCHA2D [*Thébault*, 2008] when solving for the secular variation using repeat station data. However, all solutions have the same canonical form:

$$V_{R-SCHA} = a\sum_{k\geq m}\sum_{m\geq 0} \cdot \left(\frac{a}{r}\right)^{n_k+1}\left(g_{n_k}^{i,m}\cos(m\varphi) + h_{n_k}^{i,m}\sin(m\varphi)\right)P_{n_k}^{m}(\theta) + a\sum_{k\geq m}\sum_{m\geq 0}\left(\frac{r}{a}\right)^{n_k}\left(g_{n_k}^{e,m}\cos(m\varphi) + h_{n_k}^{e,m}\sin(m\varphi)\right) \cdot P_{n_k}^{m}(\theta) + a\sum_{p\geq 0}\sum_{m\geq 0}R_p(r) \cdot \left(g_p^{m}\cos(m\varphi) + g_p^{m}\sin(m\varphi)\right)K_p^{m}(\theta) \quad (2)$$

[6] Compared to SCHA, R-SCHA involves an extra set of basis functions $K_p^{m}(\theta)$, known as Mehler functions, but uses only one set of Legendre basis functions. p is an ordering integer index. R_p are radial functions that represent the radial variation of the magnetic field inside the conical domain, provided that data are available at different altitudes. Any potential field radial function of the form $(a/r)^n$, with $n \in \mathbb{Z}$ can be expressed as a Fourier expansion upon these functions. R-SCHA2D works only for data measured at comparable altitudes, apart from this particular solution, R-SCHA solutions form a complete orthogonal basis on the interval limited by the upper and lower surfaces. The difference between R-SCHA and R-SCHA2D lies in the choice of the Mehler and the radial functions in equation (2). Compared to SCHA, R-SCHA and R-SCHA2D are mathematically complete solutions that turns to be equivalent to global spherical harmonics when the series expansion is infinite. SCHA does not satisfy this equivalence, as will be seen below.

[7] However, SCHA continues to be widely used when merging satellite and near-surface data [*Hitchman and Lewis*, 2007; *Kotzé et al.*, 2007], and when developing models using single-surface measurements [*Gaya-Piqué et al.*, 2008]. Some questions arise from these studies. Were SCHA limits properly evaluated and what is the influence of the modeling technique on them? Our purpose is thus to compare SCHA and R-SCHA from a theoretical point of view and through applied examples. The considered case studies are close to real cases, including data noise and realistic configurations from near-surface to satellite altitudes. The incompatibility between ground data and satellite data is also explored. These tests are limited to internal field vector data, and mainly

restricted to lithospheric field as SCHA diverged for other cases.

[8] The objective of this paper should be placed in the context of the forthcoming European Swarm satellite mission [*Friis-Christensen et al.*, 2006], foreseen for 2010, and the World Digital Magnetic Anomaly Map project [*Korhonen et al.*, 2007]. The possibility of merging satellite data and near-surface data opens a new range of opportunities for the study of the crustal field and regional analysis will certainly become a regular activity in the forthcoming years. The choice of the analyzing technique will be of crucial importance to recover the full spectral range of the magnetic signal.

2. Known Theoretical Limits in SCHA

[9] Both SCHA and R-SCHA have limitations in their practical applications. When looking into the SCHA scientific literature these problems are sometimes underestimated [*Torta et al.*, 2006] although it is essential to keep them in mind in order to avoid wrong geophysical interpretations.

2.1. Long-Wavelength Representation

[10] Long-wavelength modeling, like secular variation [*Korte and Haak*, 2000; *Korte and Holme*, 2003] or solar quiet variation representation [*Torta et al.*, 1997; *Gaya-Piqué et al.*, 2008] has been carried out with SCHA. *De Santis et al.* [1999] discussed the relationship between SCHA and spherical harmonics (SH). A special attention was given to the term g_0^0, a nonexisting term in SH. Since SCHA applications empirically proved to be more stable when this coefficient was low in amplitude, a common procedure consists in removing a reference model before applying SCHA. The incompleteness of SCHA basis functions is the origin of this important preprocessing.

[11] Consider the SCHA basis functions defined by $P_{nk}^m(\theta_0) = 0$, for instance. This carries the implicit assumption that the vertical component of the magnetic field averages out over the spherical cap [*Thébault et al.*, 2006a]. Similarly, the functions defined as $dP_{nk}^m(\theta_0)/d\theta = 0$ imply $\int_0^{2\pi} B_\theta \sin\theta_0 d\varphi = 0$ [*Thébault*, 2008]. Unless the considered magnetic field satisfies these conditions, none of the basis functions by itself is sufficient to represent the magnetic field in a general way. The fundamental reason for merging both sets of SCHA basis functions is to partly get rid of such drastic individual assumptions, which does not necessarily provide a robust and physical model. Remaining problems are traditionally overcome by enlarging the size of the cap [e.g., *Torta et al.*, 1992].

2.2. Radial Extrapolation of the Field

[12] *Haines* [1985] showed that SCHA models deteriorate with altitude. At present, this has a strong repercussion due to the increasing possibility of merging near-surface and satellite data. In practice, the coefficients $g_{nk}^{i,m}$ and $h_{nk}^{i,m}$ (considering internal potential only) are found in the least squares sense by minimizing:

$$\chi^2 = \| V_{SCHA} - V_{SH} \|^2_{\partial\Omega_b}$$

with $\partial\Omega_b$ the spherical cap domain defined by $\{0 \leq \theta \leq \theta_0,\ 0 \leq \varphi \leq 2\pi,\ r = b\}$. The solution is [*De Santis et al.*, 1999; *Thébault*, 2003, section 5.1]:

$$\begin{Bmatrix} g_{n_k}^{i,m} \\ h_{n_k}^{i,m} \end{Bmatrix} = \sum_{n=m}^{\infty} \left(\frac{a}{r}\right)^{n-n_k} A_k^{m,n} \begin{Bmatrix} g_n^m \\ h_n^m \end{Bmatrix} \tag{3}$$

where g_n^m and h_n^m are the SH Gauss coefficients, n and m the integer degree and order, and $A_k^{m,n}$ a transformation matrix, independent of r, equal to identity if $n_k = n$. SCHA coefficients are therefore altitude-dependent and multilevel data sets cannot be simultaneously modeled. Similarly, a model obtained at a given altitude can hardly be extrapolated to other altitudes. This issue is less prominent (although not negligible) when dealing with larger caps because $n_k \rightarrow n$ when $\theta_0 \rightarrow \pi$.

2.3. Internal-External Field Separation

[13] *Torta et al.* [1992] found that both internal and external coefficients improved the fit to a synthetic internal field input data set. When studying equivalent current systems over Europe, *Torta and De Santis* [1996] showed that internal and external coefficients, when used separately, were not able to properly describe the respective contributions. Again, an acceptable accuracy was obtained with an artificially large cap, i.e., larger than the area covered by the available data.

[14] An analytical illustration of these results could be the following one: at two surfaces $r = a$ and $r = b$, with $b > a$, the system of equations defined by (3) has no solution unless $b = a$ or $b = \infty$. We therefore must consider also $g_{nk}^{e,m}$ to obtain a system with two equations and two unknowns. In spite of the internal origin of the magnetic field, both

internal and external coefficients are necessary (but not sufficient, as SCHA is incomplete) to fit data obtained at different altitudes. The physical meaning of internal and external coefficients is thus not straightforward.

2.4. Compromise in the Simultaneous Fit of H and Z

[15] The basis function incompleteness translates into a theoretical impossibility to simultaneously solve for H and Z. *Torta et al.* [1992] observed that the compromise was more important for smaller caps. We propose the following explanation to this problem. Similarly to equation (3), but for Z, the solution that minimizes:

$$\chi^2 = \| Z_{SCHA} - Z_{SH} \|^2_{\partial\Omega_b}$$

is [*Thébault*, 2003, section 5.3]:

$$\begin{Bmatrix} g^{i,m}_{n_k} \\ h^{i,m}_{n_k} \end{Bmatrix} = \sum_{n=m}^{\infty} \left(1 + \frac{n-n_k}{n_k+1}\right) \left(\frac{a}{r}\right)^{n-n_k} A^{m,n}_k \begin{Bmatrix} g^m_n \\ h^m_n \end{Bmatrix} \quad (4)$$

[16] Comparing equation (4) with (3) drives us to the conclusion that solving simultaneously for H and Z is mathematically inconsistent. In addition, both equations diverge from each other with increasing degrees n_k. The situation improves for large caps, as n-n_k becomes small, but high-resolution modeling is not permitted.

3. Known Theoretical Limits in R-SCHA

[17] R-SCHA was developed to address SCHA shortcomings [*Thébault et al.*, 2004]. There are, however, two remaining fundamental difficulties that cannot be easily solved. The first one is related to the internal-external separation. As in SCHA, this concept cannot simply be explored by looking at the coefficients. This problem is more evident since the new Mehler coefficients g^m_p have no trivial meaning. Each set of coefficients plays a separate role within the cone: $g^{i,m}_{nk}$ coefficients are more important in the lower part of the region, while $g^{e,m}_{nk}$ are more significant in the upper part. By construction, g^m_p coefficients are dominant near the lateral edges.

[18] The second problem with R-SCHA is the series convergence rate. It is well known that Fourier-like series converge slowly toward the solution; this applies to R-SCHA (as it does with SCHA when only one set of basis functions is considered). This is no difficulty if enough data are available but can be a problem in case of inverse problems involving few data points.

4. Case Studies and Performance Comparisons

[19] Many theoretical shortcomings come along with the traditional SCHA technique, but it is necessary to compare SCHA to R-SCHA or R-SCHA2D performance in realistic cases. The purpose of this section is to investigate different cases close to reality.

[20] The synthetic examples are calculated on a cap centered at 44°N, 3°E, with 7° half-angle. Synthetic data are computed on regular grids. In most cases, the SH model used is POMME 3.1 model [*Maus et al.*, 2006], which gives an estimation of the core and crustal field up to a maximum degree $n = 90$. For some cases, a Gaussian random noise defined by $\epsilon = N(\sigma^2, 0)$ is added, with $\sigma = 5 - 4.5\ h/550$ in nT where h is the altitude of the data in km. 550 km refers to the highest altitude in km of the Swarm constellation; 4.5 nT is chosen so that the noise is 0.5 nT at 550 km altitude. For the single-surface case, R-SCHA2D [*Thébault*, 2008] was used instead of R-SCHA. In this study, we avoid regularization [e.g., *Korte and Holme*, 2003; *Thébault et al.*, 2006a]. This allows us to concentrate on the performance of the modeling basis functions themselves. For each studied case, the modeling parameters and RMS are given in Table 1.

4.1. Single Surface Problem

4.1.1. Fit to Main Field and Crustal Field

[21] Synthetic data are calculated from spherical harmonic degree $n = 1$ to $n = 90$. The fit to the main field is shown in Figure 1. As can be seen, the SCHA model developed on the 7° cap (second column) is not able to represent the input data and fictitious oscillations appear all over the region. The results were worst when going to higher expansions but reach an acceptable accuracy for a 40° cap. The expansion was limited to $K_{max} = 10$. Both results confirm the theoretical long-wavelength issues discussed above: fitting H and Z at the same time is easier with larger caps (because n_k is closer to n) but degrades with the series expansion. The best root mean square obtained (RMS) were 5.9 nT for the X component, 7.9 nT for Y, and 9.2 nT for Z.

Table 1. Modeling Parameters, Minimum Wavelength, and Residual Mean Squares for the Applied Comparisons Between SCHA and R-SCHA Considering the 7° Half-Angle Cap Discussed in the Text

	Method					
	SCHA			R-SCHA		
Parameters	Kmax	λ_{min} (km)	RMS (nT)	Kmax	λ_{min} (km)	RMS (nT)
Main field (noise free)	10	298	7.50	15	110	0.50
Main field differences (noise free)	15	201	0.07	6	370	0.02
Main field differences sparse data (noise free)	8	370	0.10	6	370	0.02
Crustal field (noise)	12	250	4.50	12	138	4.40
Crustal field (WDMAM noise free)	22	138	14.31	21	77	14.5
Crustal field (WDMAM noise free)	23	132	19.50	30	53	10.4
Crustal field (WDMAM noise free)	36	83	34.34	35	45	8.2
Swarm: multisurface coverage (noise free)	12	250	0.14	12	138	0.40
Swarm: multisurface coverage (noise)	12	250	1.80	12	138	1.90
Swarm: data gap (noise free)	12	250	0.14	12	138	0.40
Swarm: data gap (noise)	12	250	3.70	12	138	3.70
Swarm: incompatible data (noise)	12	250	2.10	12	138	2.50

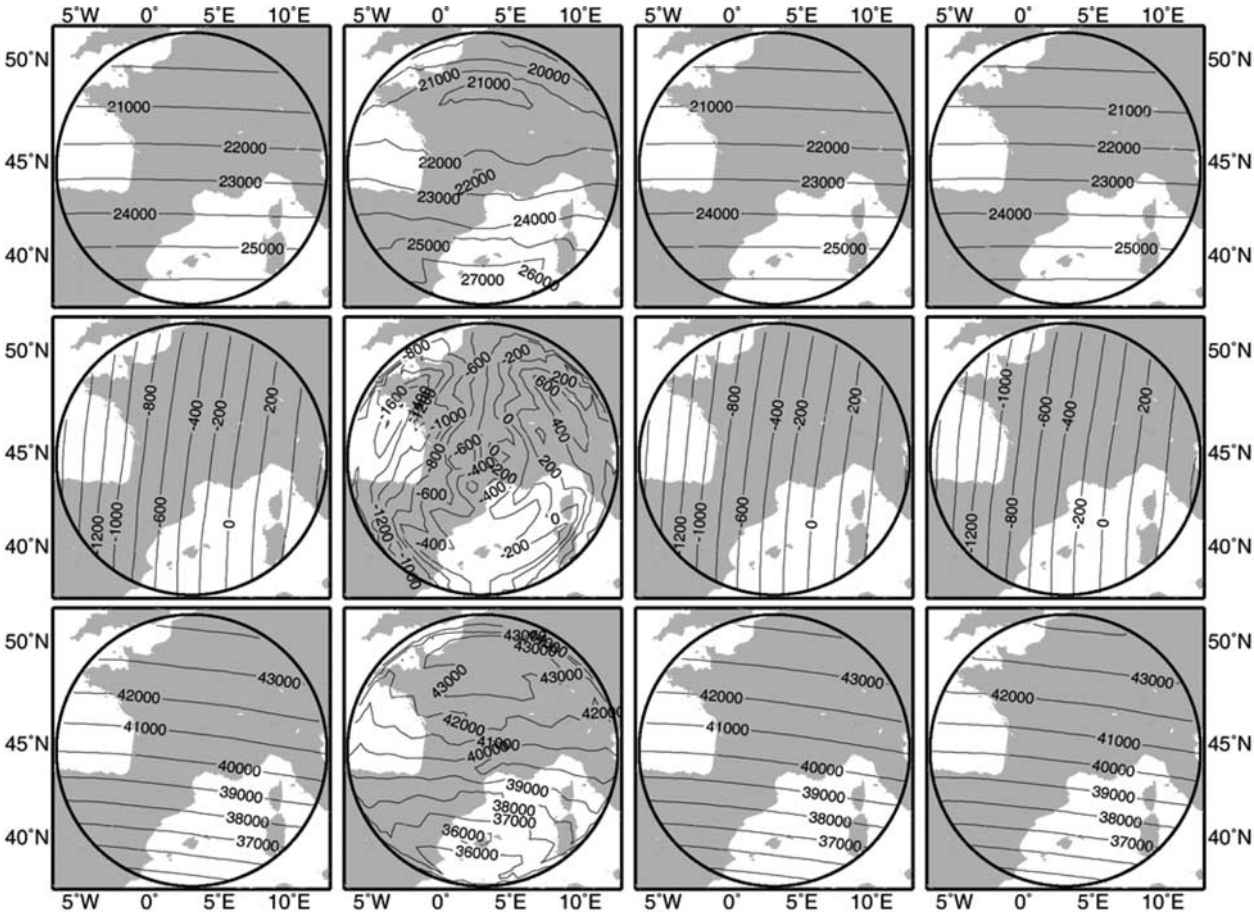


Figure 1. Modeling of POMME near-surface main field data (first column) by using SCHA (second column) and R-SCHA (third column) techniques. (top) X, (middle) Y, and (bottom) Z components. The problems presented by the SCHA technique apparently disappear when the size of the spherical cap is much larger than the area covered by data (fourth column).

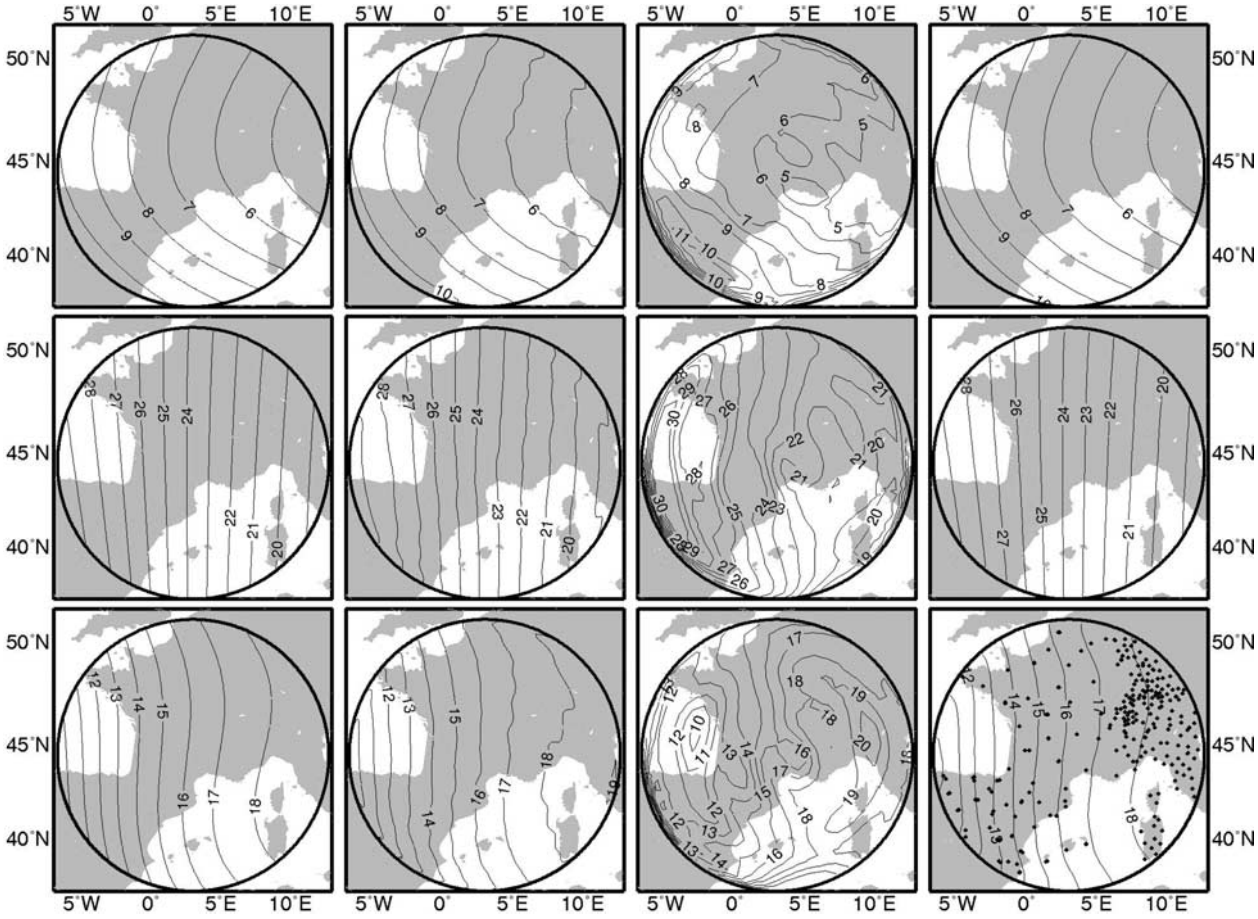


Figure 2. POMME 3.1 and 2.5 main field difference (first column), SCHA from a regular grid (second column), SCHA (third column), and R-SCHA2D (fourth column) from a real data distribution. Real data distribution is shown on the bottom right (diamonds). (top) X, (middle) Y, and (bottom) Z components.

[22] The R-SCHA approach does not need any special treatment (third column in Figure 1). For this particular model, the RMS values with respect to the input data are below 1.2 nT for Z and below 0.02 nT for X and Y for series expansion up to $K_{max} = 15$ in equation (2).

4.1.2. Fit to Main Field Differences

[23] SCHA is traditionally used after a global reference field was subtracted first from the data. This ''detrending'' is reproduced considering the difference between models POMME 3.1 [*Maus et al.*, 2006], centered at epoch 2003.0 and POMME 2.5 (http://www.gfz-potsdam.de/pb2/pb23/Models/index.html), centered at epoch 2002.5. for degrees 1 to 15. It is equivalent to correcting data with a 6 months old main field model.

[24] For equally distributed data SCHA performs well in terms of statistics (RMS = 0.07 nT) but the model exhibits oscillations that betray the difficulty of SCHA to simultaneously fit the three components (Figure 2). In fact, the inverse problem is already unstable.

[25] Ground data are usually sparsely distributed. This case is analyzed using repeat station and observatory data inside the cap between 1965 and 2003. The POMME models difference is used again. Data location are obtained at the World Data Center, Edinburgh and the series expansions are adjusted considering the real data distribution (see Table 1). SCHA fits well the data but the model calculated on a regular grid is very noisy.

[26] The parameter correlation between these two cases is 0.5. R-SCHA2D also fits well the data and predicts correctly the field outside the data loca-

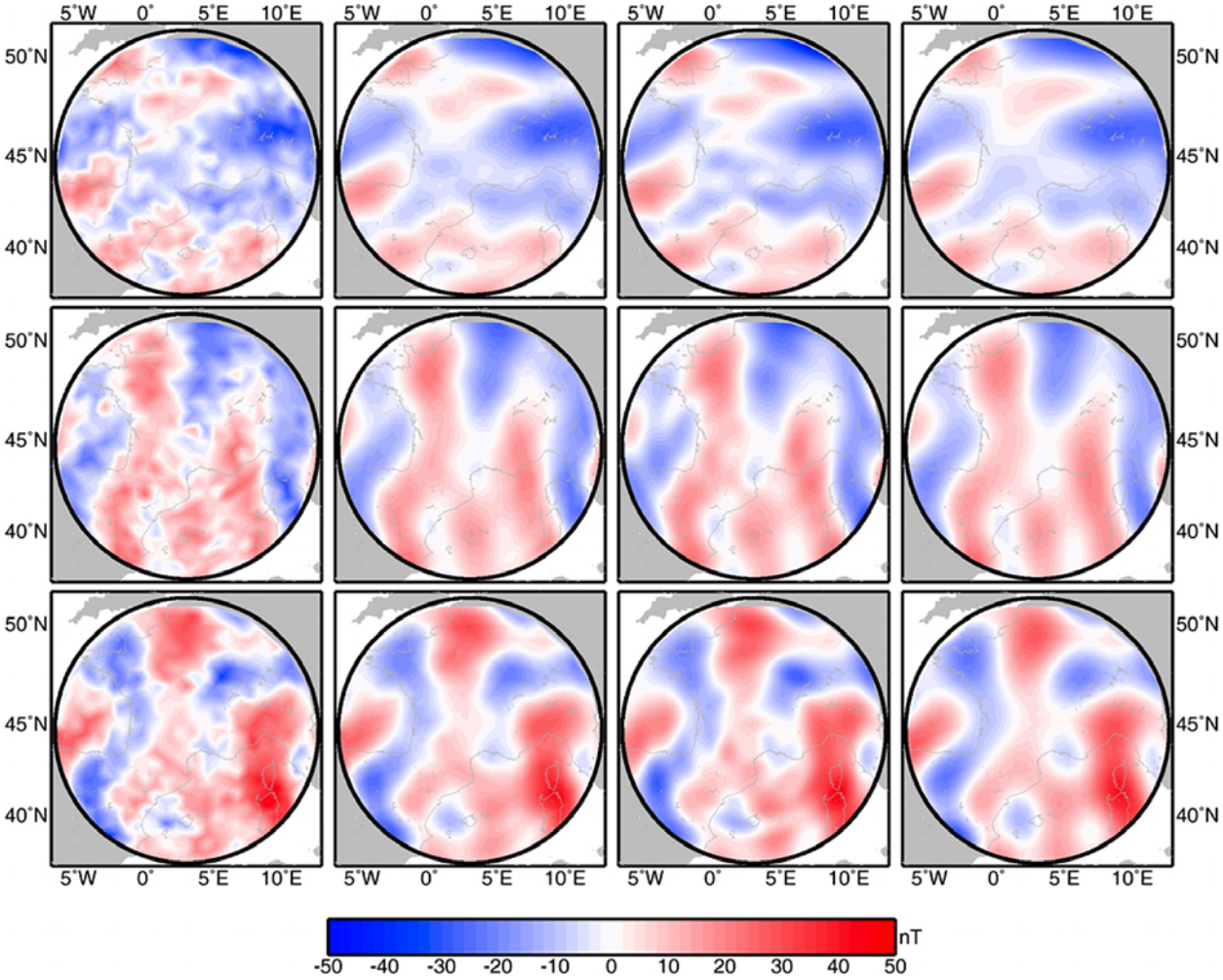


Figure 3. Modeling of POMME near-surface crustal field noisy data (first column) by using SCHA (second column) and R-SCHA (third column) techniques. (top) X, (middle) Y, and (bottom) Z components. Noise-free data are shown in the fourth column.

tion. The parameter correlation between the two cases is 0.99 for R-SCHA2D.

4.1.3. Fit to Long-Wavelength Crustal Field

[27] This third test is carried out with noisy data (Gaussian noise) calculated from degrees $n = 15$ to $n = 90$ of POMME3.1. For lithospheric fields, it is not necessary to increase the size of the spherical cap in SCHA (Figure 3). Removing degrees $n = 1$ to 14 is efficient and reduces the problem of misfit between H and Z. RMS values are 4.6, 4.7, and 4.4 nT for X, Y, and Z components, respectively. These values are comparable to R-SCHA2D statistics (4.1, 4.2, and 3.7 nT, respectively). It can therefore be concluded that both SCHA and R-SCHA2D techniques are statistically equivalent in the case of single-surface large wavelengths crustal field modeling, being both able to model the input data up to the noise level.

4.1.4. Fit to Long- and Medium-Wavelength Crustal Field

[28] We now use a SH model from degree n = 12 to 600 representing a minimum wavelength of 67 km at the Earth's surface (NGDC-720, http://www.ngdc.noaa.gov/geomag/EMM/emm.shtml). It is based on the World Digital Magnetic Anomaly Map [*Korhonen et al.*, 2007]. Synthetic data are calculated on a regular grid of 5352 points. Figure 4 shows that SCHA has difficulties to fit the vector data. The SCHA model is limited to a spatial resolution somewhere around 130 km (see Table 1). Going to higher series expansion leads

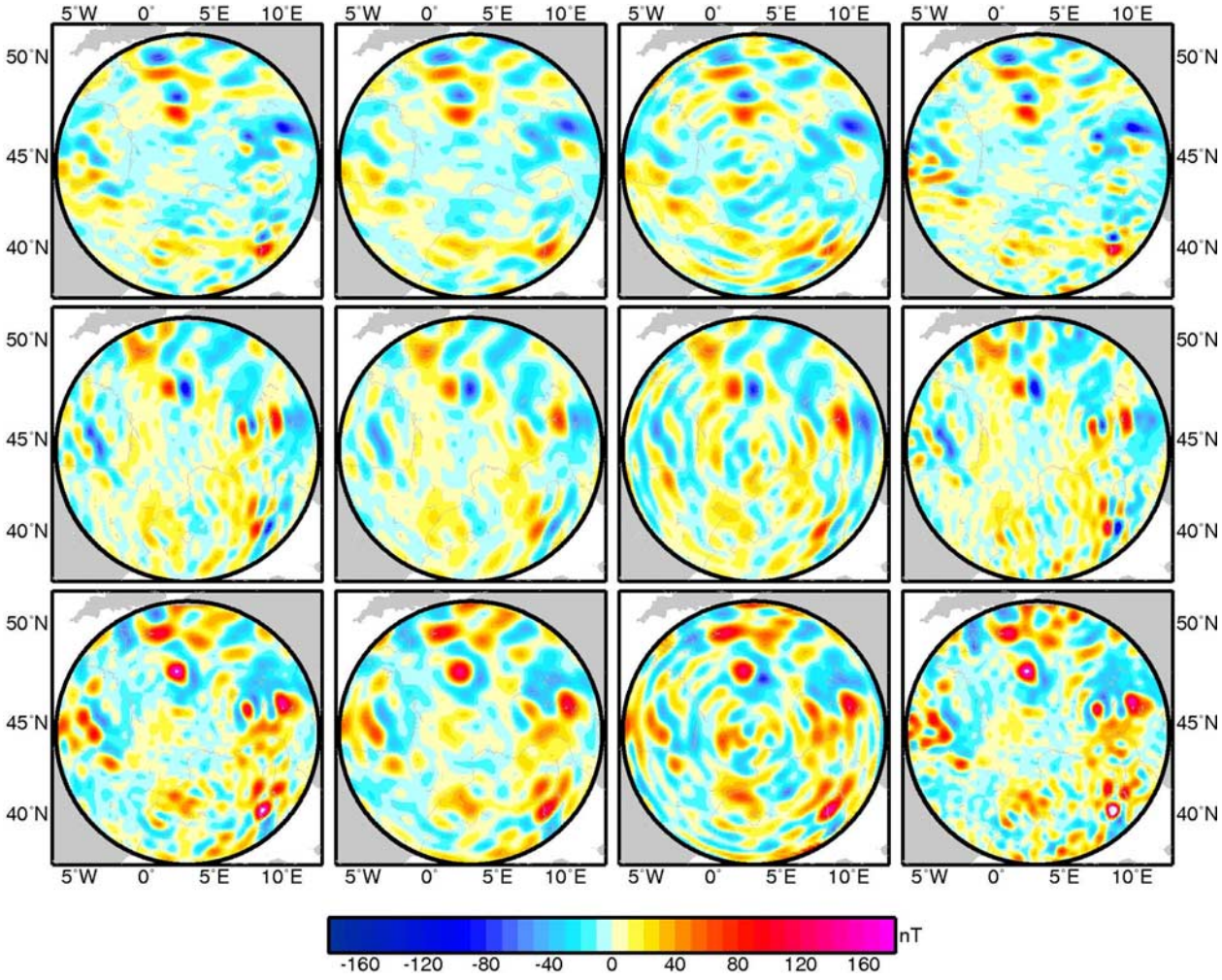


Figure 4. Modeling of NGDC-720 near surface crustal field (first column). SCHA model at 138 km (second column) and 132 km (third column) resolution. R-SCHA2D model at 45 km resolution (fourth column). (top) X, (middle) Y, and (bottom) Z components.

to unstable SCHA (note the increase of RMS with Kmax in Table 1). This confirms the fit problem between the H and Z components. For high series expansion, equations (3) and (4) diverge from each other. SCHA is thus band limited between wavelengths shorter than the size of the cap but greater than some minimum wavelength imposed by numerical limitations. R-SCHA2D converges slowly but the data are represented to their resolution.

4.2. Multisurface Problem

[29] The Swarm mission will provide the best ever survey of the Earth's magnetic field between 350 and 550 km altitude [e.g., *Olsen et al.*, 2006]. In this section we compare SCHA and R-SCHA on a data set that mimics the multisatellite Swarm configuration. Figure 5 shows the data distribution with values at the mean Earth's radius, between 350 and 450 km altitude at 20 km interval, and between 500 and 550 km at 10 km spacing. From now on, synthetic data are calculated from spherical harmonic degree 15 to 90.

4.2.1. Swarm-Like Distribution: Complete Multisurface Coverage

[30] Figures 6–8 present the residual between noise-free data and SCHA (second column) or R-SCHA (third column) for the three components at different altitudes. SCHA performs better in this case. R-SCHA models have edge effects due to the poor radial data coverage. Mehler functions in equation (2) are not very well constrained. Regu-

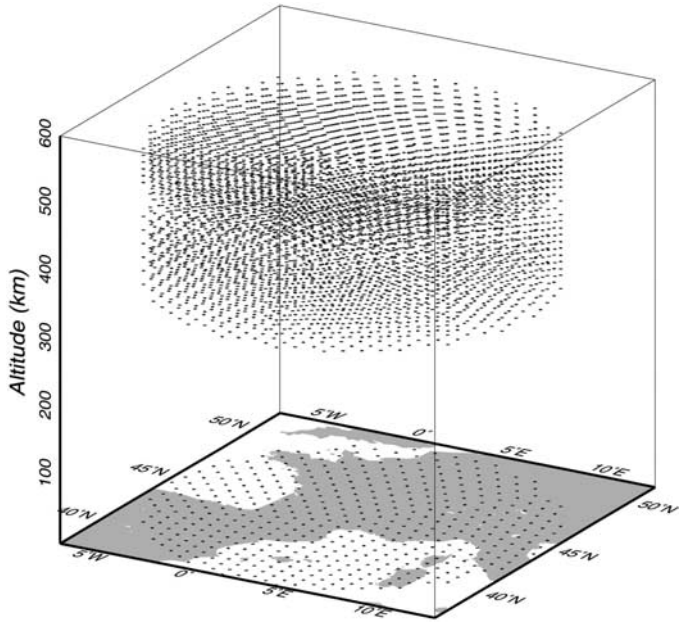


Figure 5. Locations where the POMME model has been calculated for the multilevel tests with a data gap between 0 km and 350 km altitude.

larization is needed to reduce these oscillations. Although this is a common procedure [e.g., *Haines and Torta*, 1994; *De Santis et al.*, 1996; *Korte and Holme*, 2003], the purpose of this manuscript being to objectively compare both technique, we avoided regularization.

[31] When noise is added (Figures 9–11), both SCHA (second column) and R-SCHA (third column) models fit the data (first column) to the noise level (shown in the fourth column for comparison). Only fit up to 200 km is shown since both models look equivalent beyond that altitude. In the case of lithospheric field noisy data R-SCHA and SCHA are almost equivalent, even though R-SCHA converges slower (see Table 1).

4.2.2. Swarm-Like Distribution: Data Gap at the Earth's Surface

[32] Besides the Swarm mission, other contemporary initiatives are contributing to improve our knowledge of the magnetic field. Among them, the World Digital Magnetic Anomaly Map (WDMAM) project is an international effort to merge together available aeromagnetic compilations and near-surface magnetic anomaly data [*Korhonen et al.*, 2007]. However, current compilations and data do not cover all areas in the world. In this comparison, a region devoid of data at the surface is considered (Figure 12, bottom left). Satellite altitudes are well covered.

[33] In the case of noise-free data (Figures 12–14), SCHA fits the data properly and interestingly predicts fairly well the field inside the gap region. For the R-SCHA model (residuals shown in the third column) fictitious oscillations appear not only at the surface but extend up to 200 km with important border effects. However, the fit of the SCHA model becomes extremely bad (residuals above 400 nT) when noise is added to the data (Figures 15–17). SCHA estimated coefficients show large differences between noise and noise-free data modeling. The correlation between both sets of coefficient is 0.60. To the contrary, the R-SCHA model gives approximately the same results in both cases. The correlation between the two sets of parameters is 0.99. In a real noisy data situation,

Figure 6. Modeling of POMME multilevel crustal field data (first column). Residuals between data and SCHA (second column) and between data and R-SCHA (third column) techniques, from 0 km (sixth row) to 500 km (first row) at 100 km interval. X component.

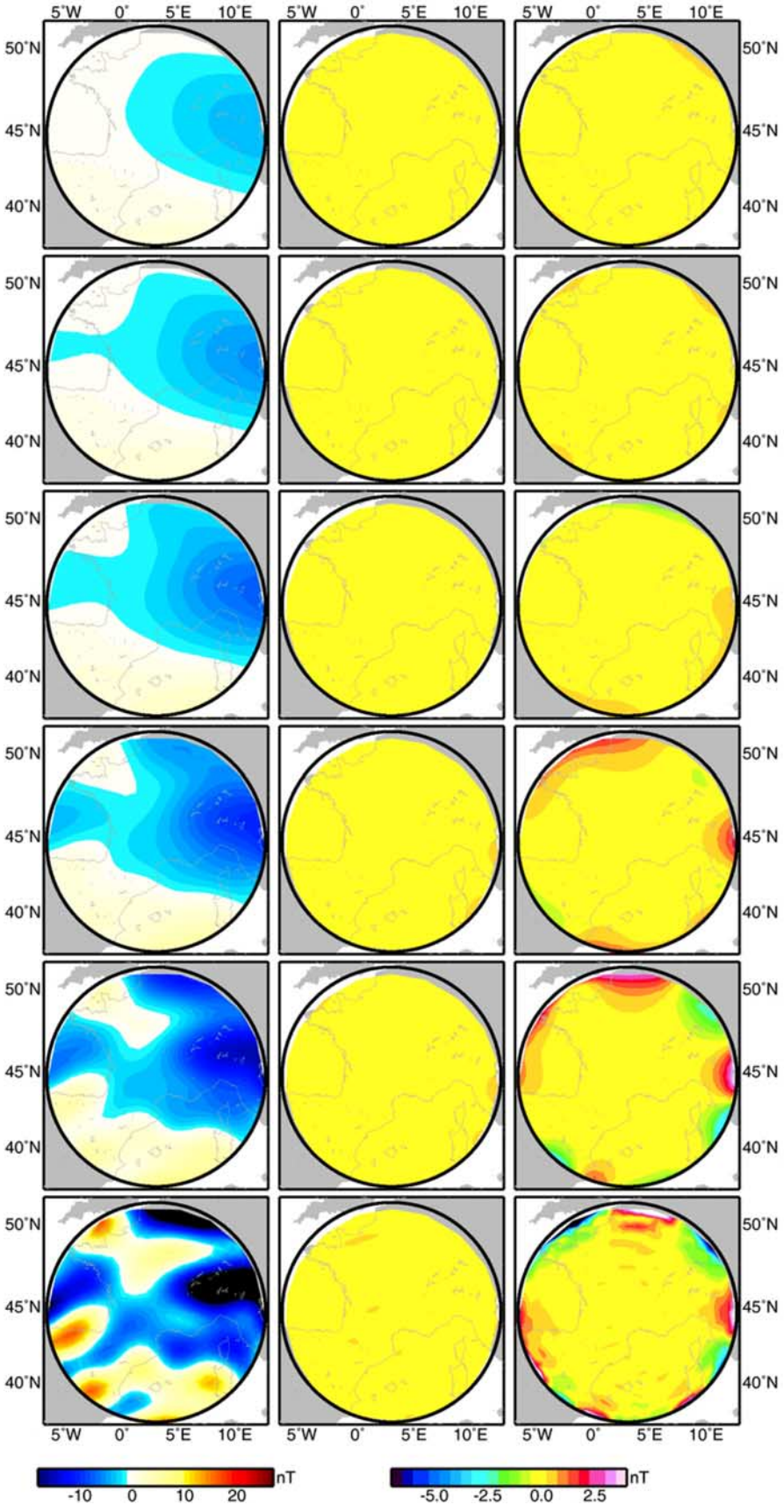


Figure 6

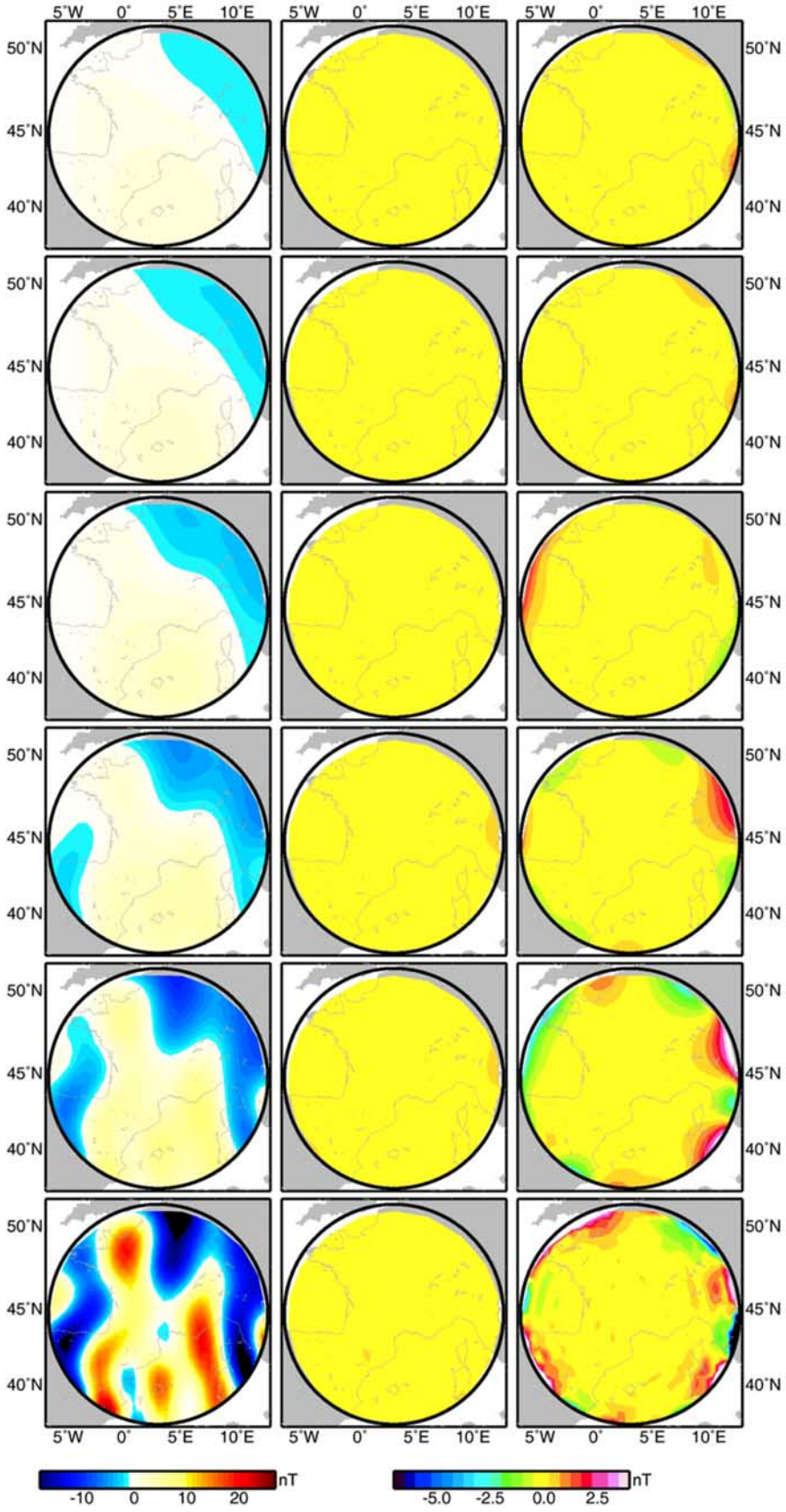


Figure 7. Same legend as in Figure 6 for Y.

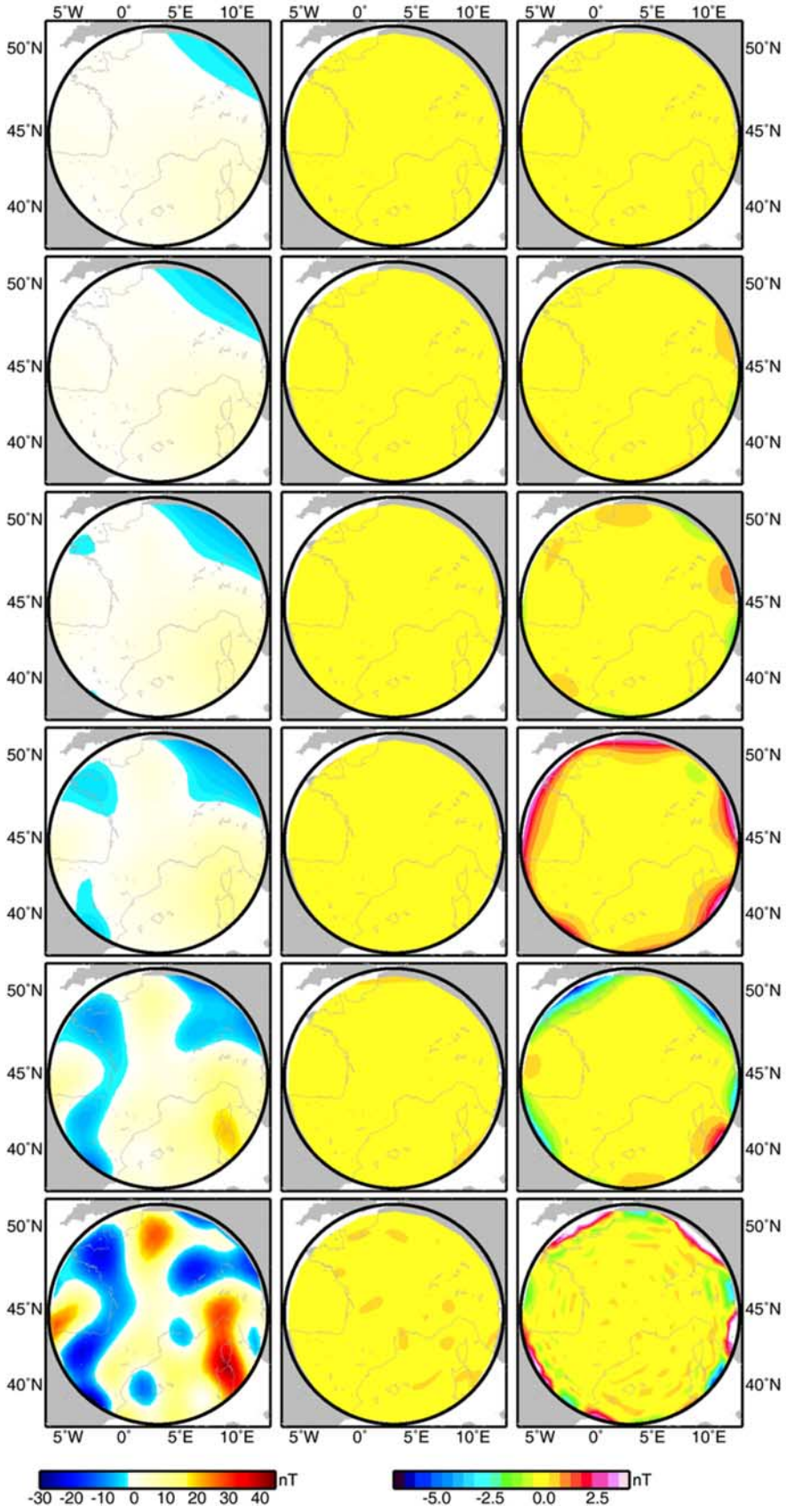


Figure 8. Same legend as in Figure 6 for Z.

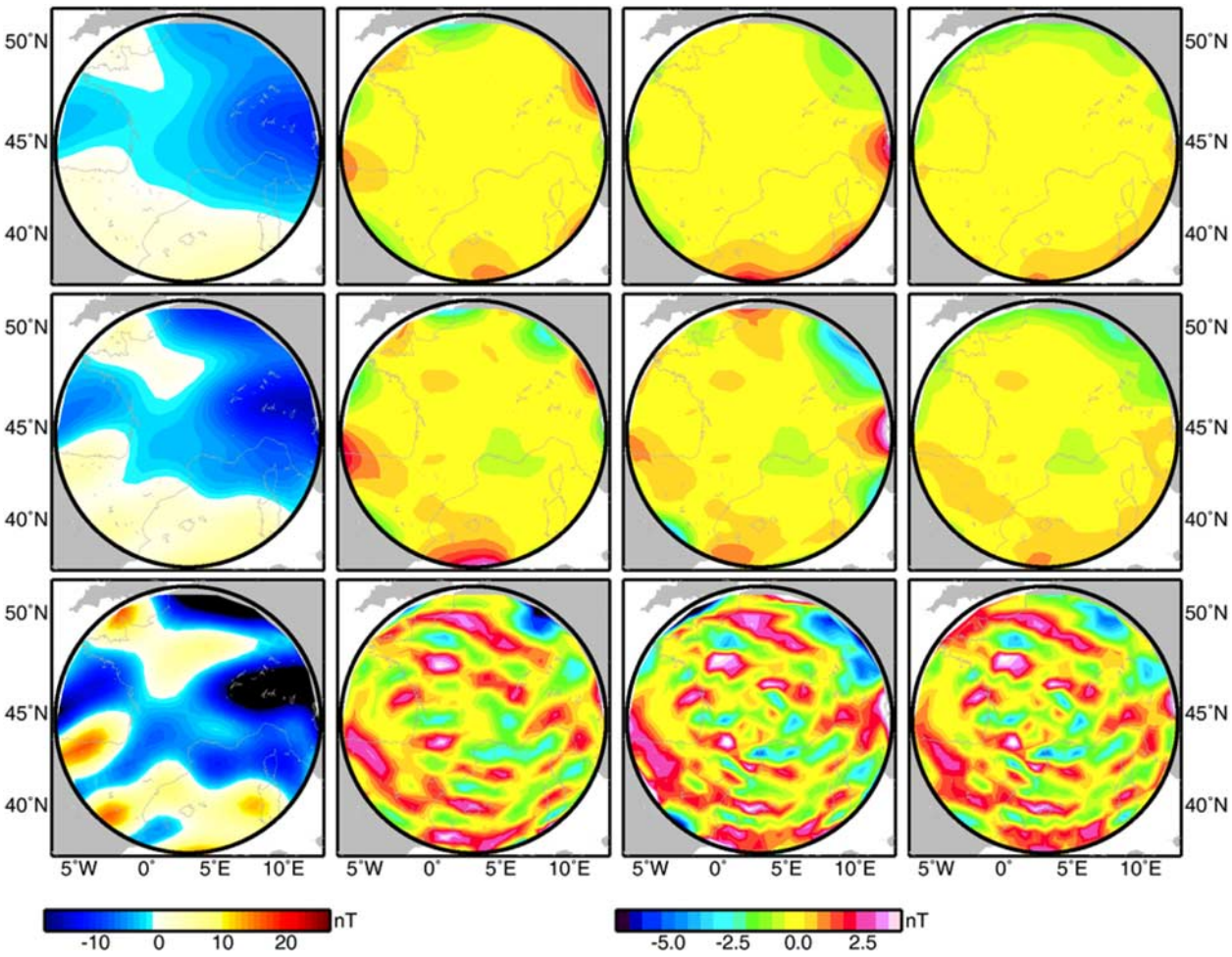


Figure 9. Modeling of POMME multilevel crustal field noisy data (first column). Residuals between data and SCHA (second column) and between data and R-SCHA (third column) techniques, at (bottom) 0 km, (middle) 100 km, and (top) 200 km. The fourth column shows the added random noise. X component.

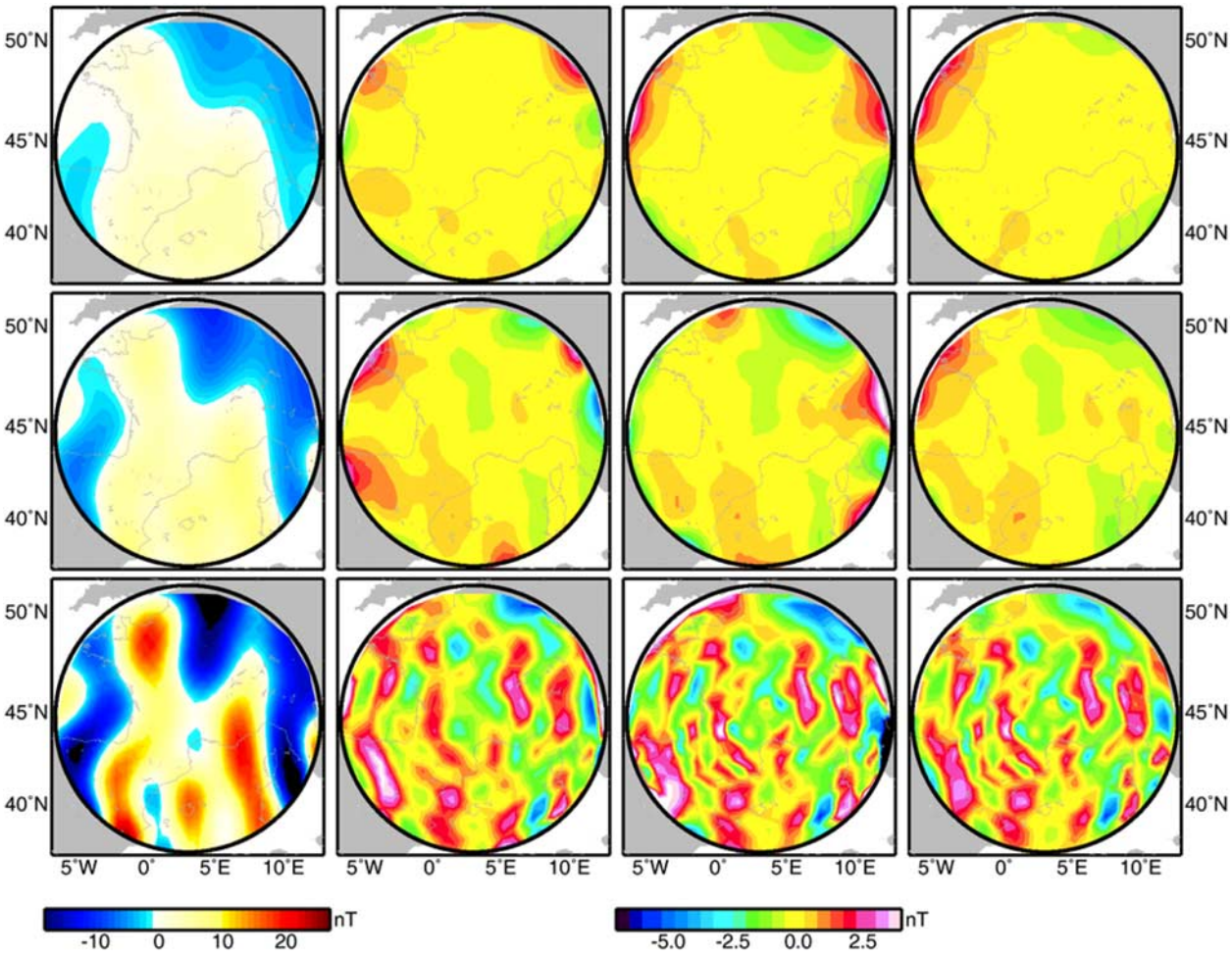


Figure 10. Same legend as in Figure 9 for Y.

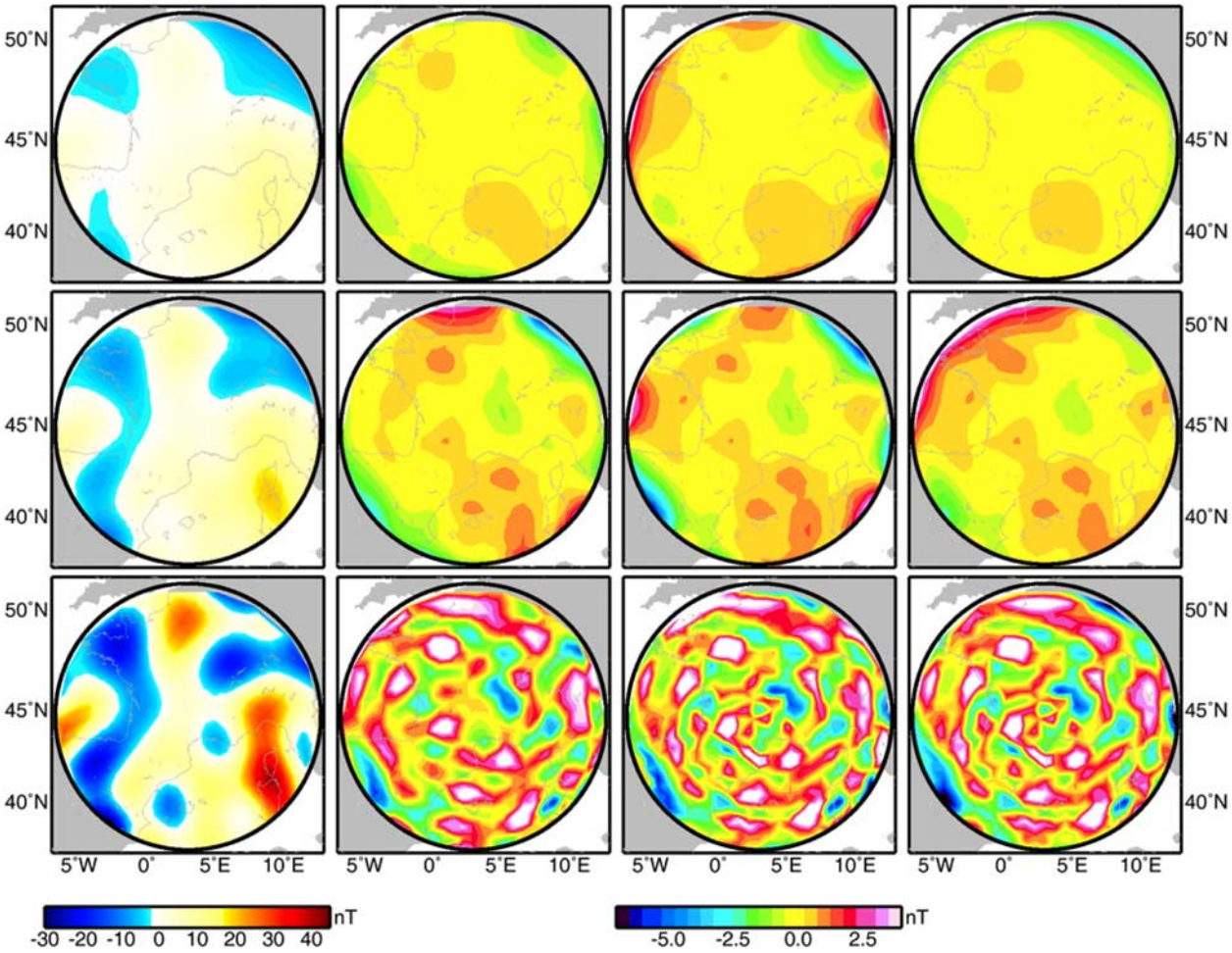


Figure 11. Same legend as in Figure 9 for Z.

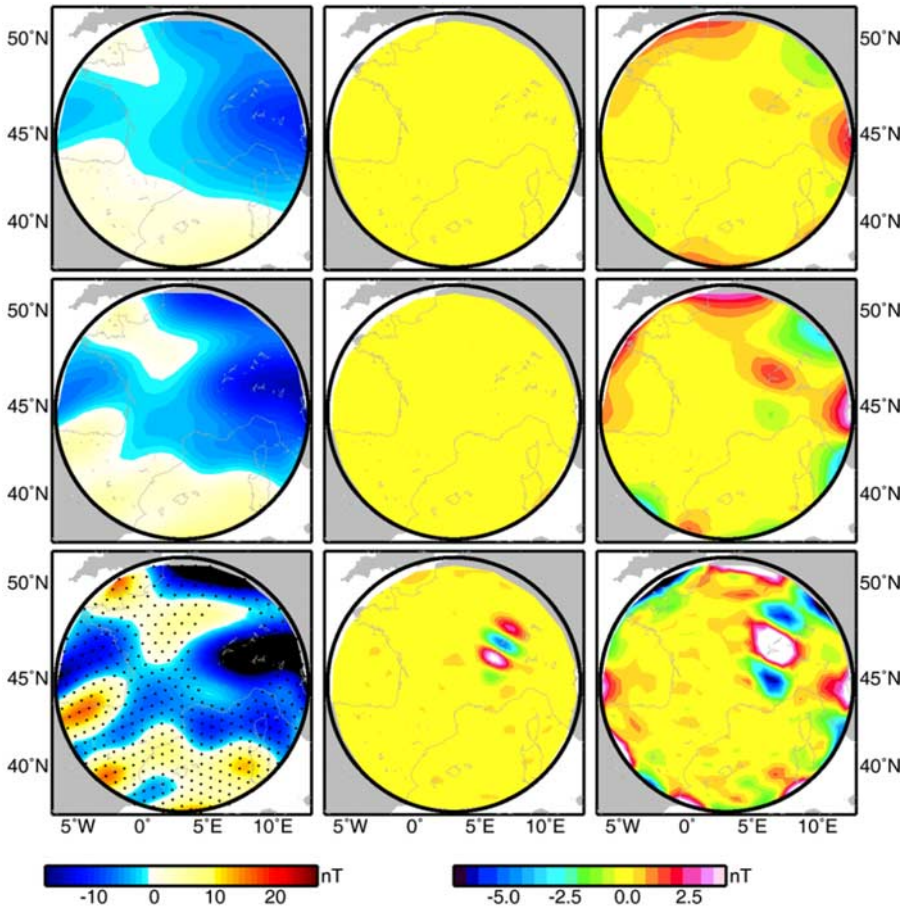


Figure 12. Modeling of POMME multilevel crustal field data with a subregion devoid of near-surface measurements (first column). Residuals between original synthetic model (first column) and SCHA (second column) and between original synthetic model and R-SCHA (third column) techniques, at (bottom) 0 km, (middle) 100 km, and (top) 200 km. X component.

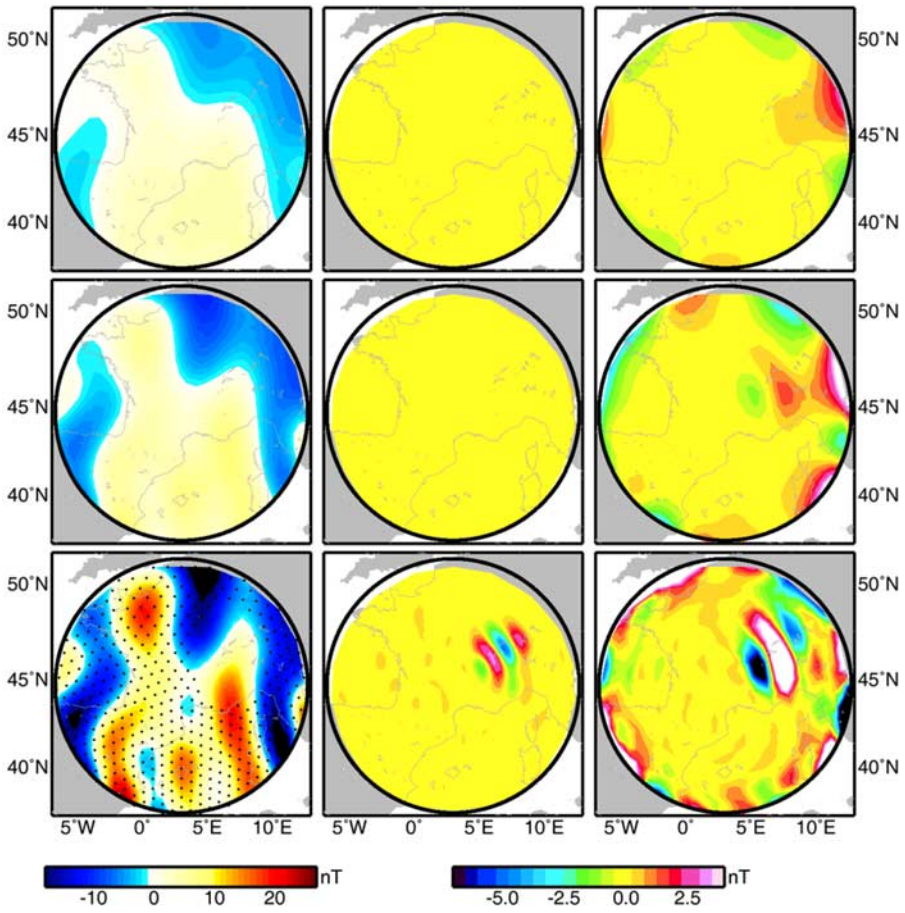


Figure 13. Same legend as in Figure 12 for Y.

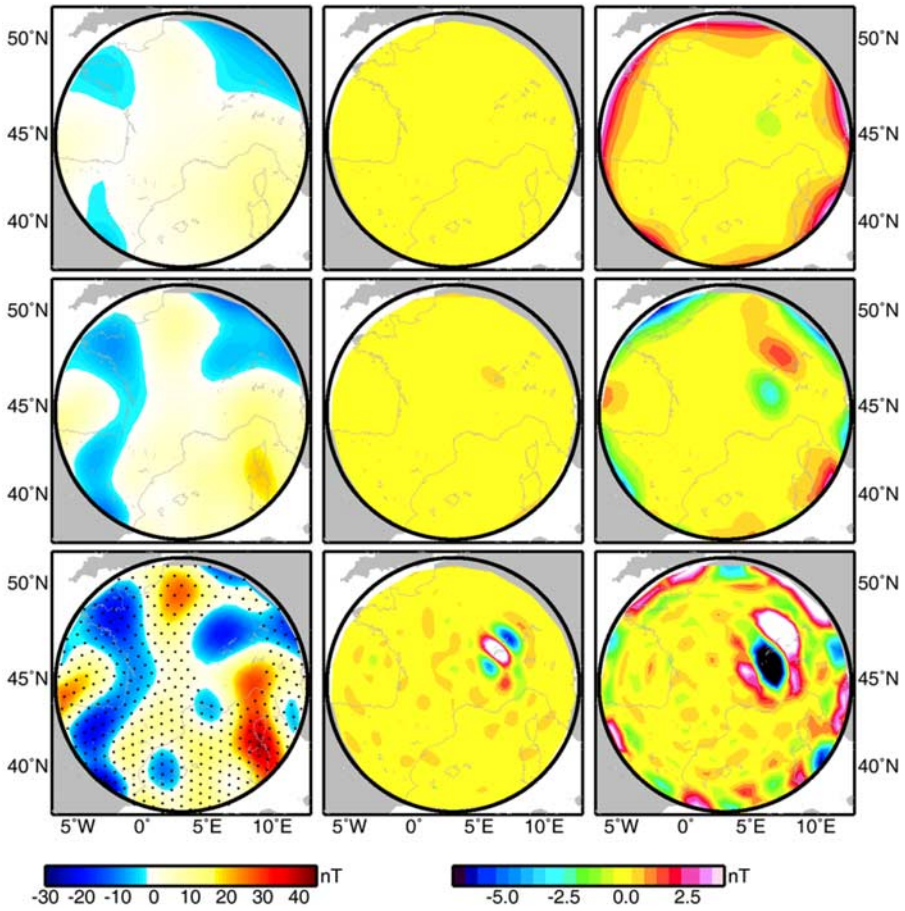


Figure 14. Same legend as in Figure 12 for Z.

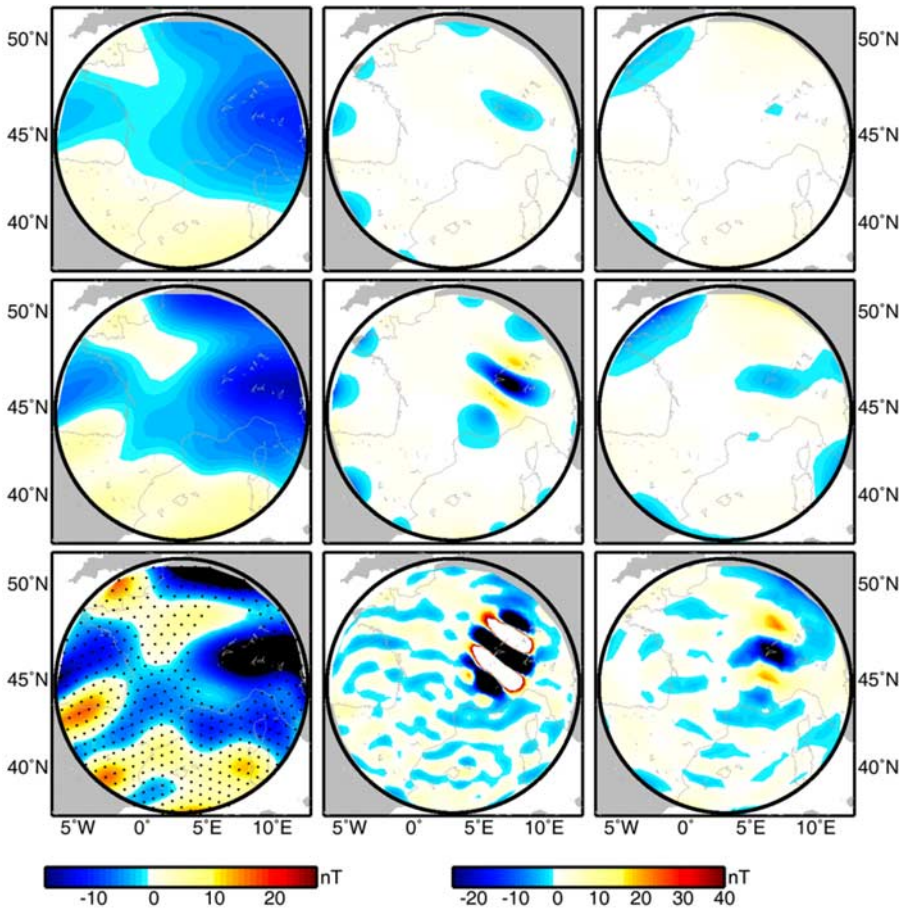


Figure 15. Modeling of POMME multilevel crustal field data with a subregion devoid of near-surface measurements (first column). Residuals between synthetic model with noise (first column) and SCHA (second column) and between original synthetic model and R-SCHA (third column) techniques, at (bottom) 0 km, (middle) 100 km, and (top) 200 km. X component. The noise is shown in Figure 9.

R-SCHA converges slower than SCHA but is more stable inside data gaps.

4.2.3. Swarm-Like Distribution: Incompatible Surface and Satellite Data

[34] Another very likely situation is having to deal with incompatible data. All nonlithospheric field contributions contaminate data in very different ways [e.g., *Hamoudi et al.*, 2007] and long-wavelength near-surface and satellite data are usually incompatible [e.g., *Ravat et al.*, 2002]. In order to investigate this situation, ground synthetic data are calculated with the lithospheric field model (up to n = 150) used to carry out the End-to-End Plus simulator of the forthcoming Swarm mission [*Olsen et al.*, 2007]. The synthetic Swarm model and POMME have a spherical harmonic degree correlation degrading with the degree.

[35] The results in Figures 18–20 are eloquent. While R-SCHA has the correct behavior and does not adjust to incompatible data (third column), SCHA fits the data with an average error below 5 nT. If noise were added, this aspect of SCHA would not have been detected. Note that if R-SCHA residuals are higher at the lowest surface it is because we have more satellite than near-surface data. In a real situation residual field data are partially incompatible as a result of different processing techniques applied to the original measurements. This shows that in the case of highly incompatible data SCHA models have inconsistent spatial spectral content while R-SCHA will poorly fit the data.

5. Conclusions and Discussion

[36] Most theoretical issues discussed in this paper are confirmed when performing synthetic inverse

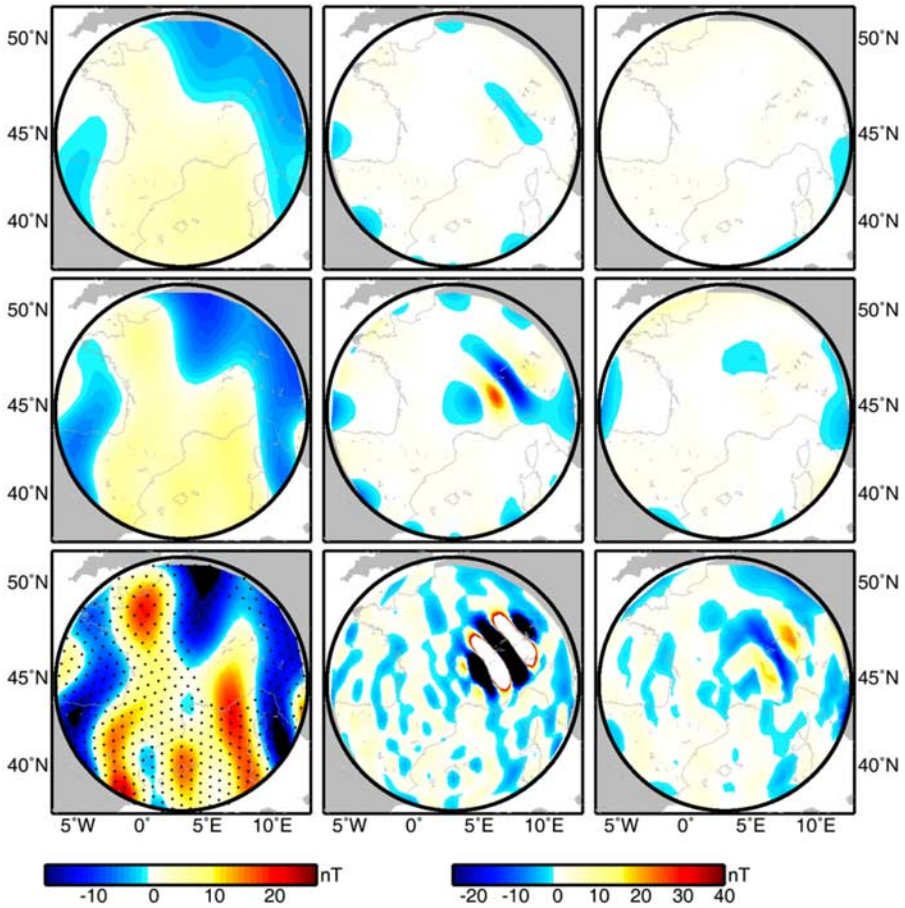


Figure 16. Same legend as in Figure 15 for Y. The noise is shown in Figure 10.

problems. SCHA and R-SCHA regional modeling techniques have been compared by checking the output models with different data sets and scenarios. When considering near-surface main field data, SCHA does not work correctly. When considering a partial detrending (i.e., removing an incomplete main field), SCHA behaves better but shows unrealistic small scales oscillations for perfectly distributed data and it is rather unstable in a real data distribution situation. Realistic SCHA results are obtained within a band limited spectral domain. It is not permitted to expand the series to very high degree with SCHA and thus, to represent high-resolution data. For the cap size analyzed here, the model is stable between wavelengths λ_{max} = 2500 km and λ_{min} = 130 km considering an ideal data distribution.

[37] Further work was carried out within this band limited spectral region to compare SCHA and R-SCHA using a data distribution close to the forthcoming Swarm satellite mission. The full illustration of the R-SCHA multilevel data performance would have consisted in considering the total field, a situation not permitted by SCHA. The multilevel problem applied to noise-free data showed that SCHA converges faster than R-SCHA. R-SCHA requires comparatively higher series expansion. In the absence of regularization, R-SCHA technique slightly suffers from spurious oscillation of the radial functions that are not well constrained with the Swarm configuration. It also comes out that R-SCHA and SCHA become statistically equivalent in the case of noisy synthetic lithospheric field data.

[38] When a gap is present in the data distribution at the Earth's surface, the result is more surprising. In the case of perfect data, SCHA seems superior to R-SCHA in terms of fit and gap prediction. This is due to the redundancy of SCHA basis function that increases the rate of convergence of the solution, but at the cost of the modeling parameters presenting aberrant values. It is important to keep in mind

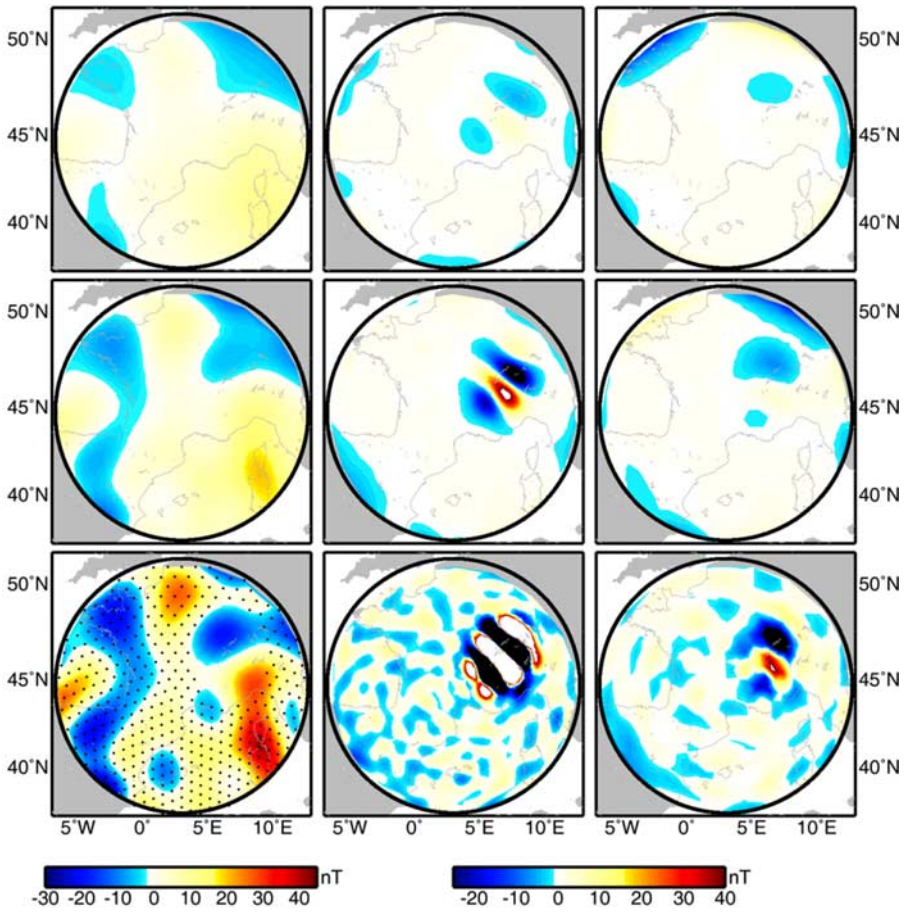


Figure 17. Same legend as in Figure 15 for Z. The noise is shown in Figure 11.

that the inverse problem statistics does not ensure the stability of the model. In the case of noisy data, the prediction by SCHA is much worse than that by R-SCHA. The SCHA basis functions being not orthogonal, the conditioning of the inverse problem is particularly bad in the case of data gaps. As a result, the whole set of parameters exhibits completely new values. The convergence for R-SCHA models is slower, but the parameter estimation is robust and less dependent on noise or gap. Most important was the case of incompatible data analysis. It seems that SCHA assimilates all data, whatever their respective level of compatibility. To the contrary, R-SCHA does not adjust to incompatible data. This is an important result as, in a real situation, near-surface data are often acquired with different platforms, at different times with different devices. Incompatibility between satellite and near-surface is a very common problem [e.g., *Ravat et al.*, 2002]. If regional models are used to infer hypothesis about source depth and geometry, we should be ascertained that the technique employed generates self-consistent models at all wavelengths.

[39] Some very simple procedures, like the statistical or physical regularization may from time to time improve the reliability of SCHA models. However, when evaluating a technique it is important to consider other aspects, not discussed in details here, like the conditioning of the inverse problem and parameter stability. In this regard, R-

Figure 18. Modeling of incompatible data (first column) using POMME between 350 and 550 km altitude and a Swarm synthetic model. Residuals between data and SCHA (second column) and between data and R-SCHA (third column) techniques from 0 km (sixth row) to 500 km (first row) at 100 km interval. X component.

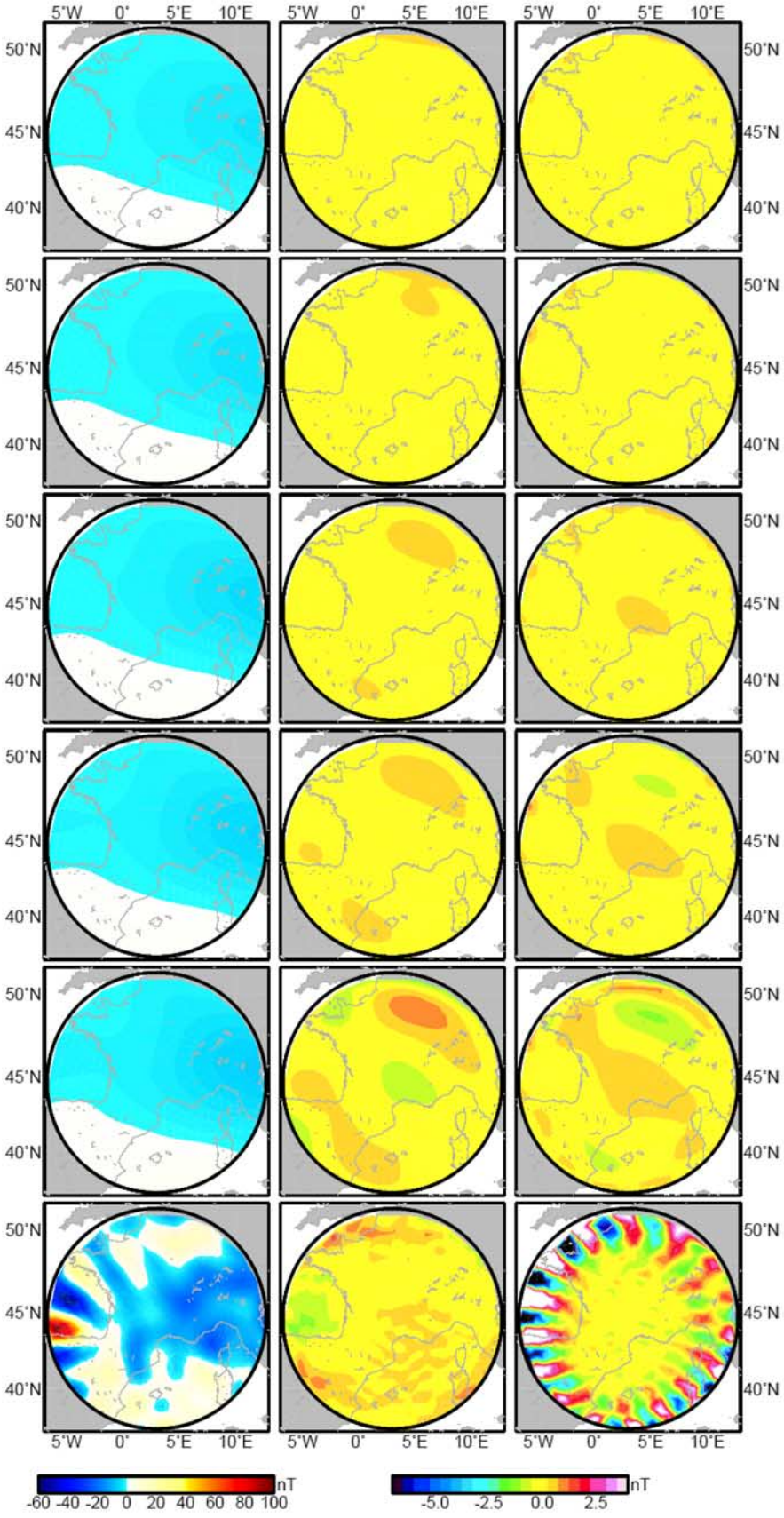


Figure 18

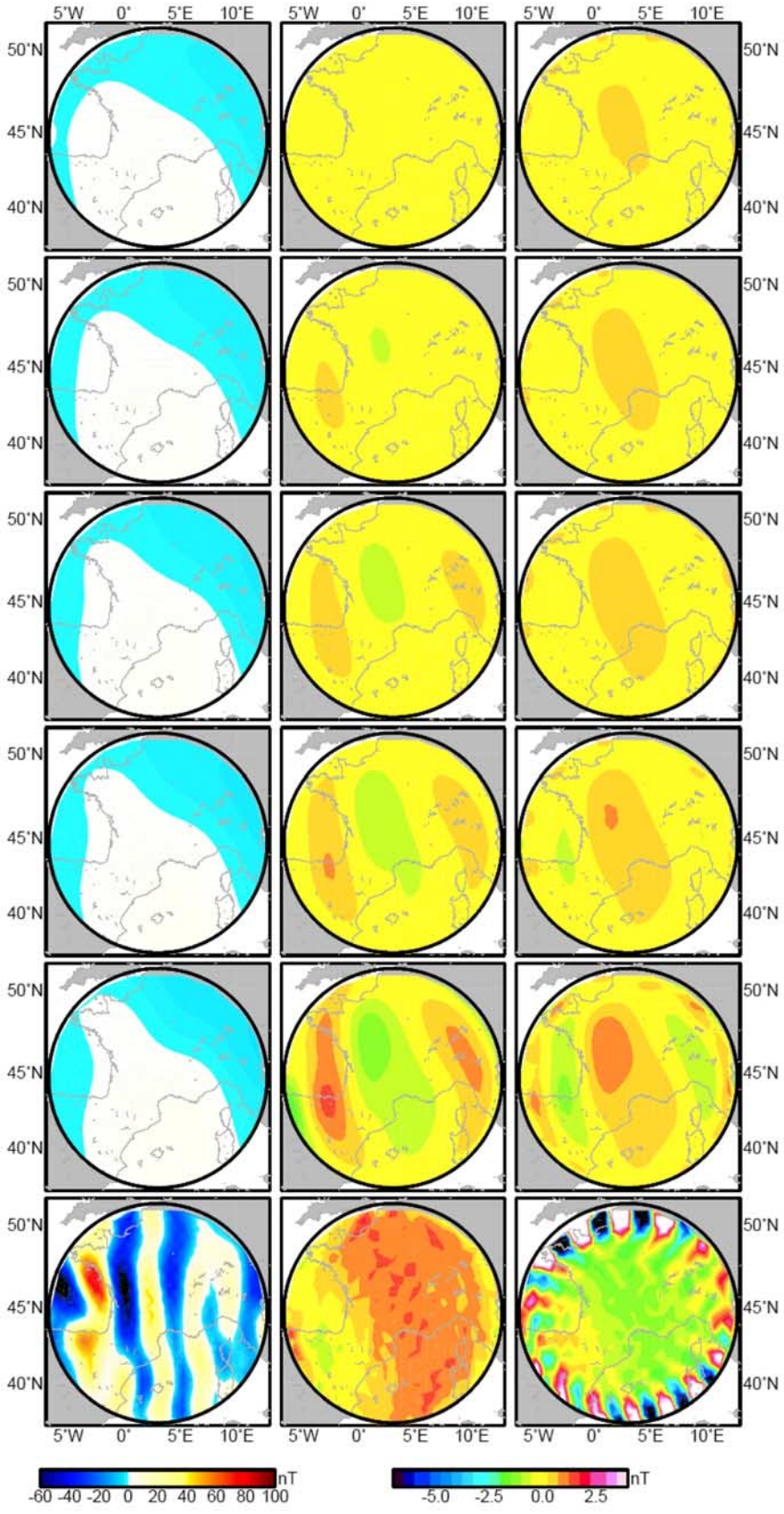


Figure 19. Same legend as in Figure 18 for Y.

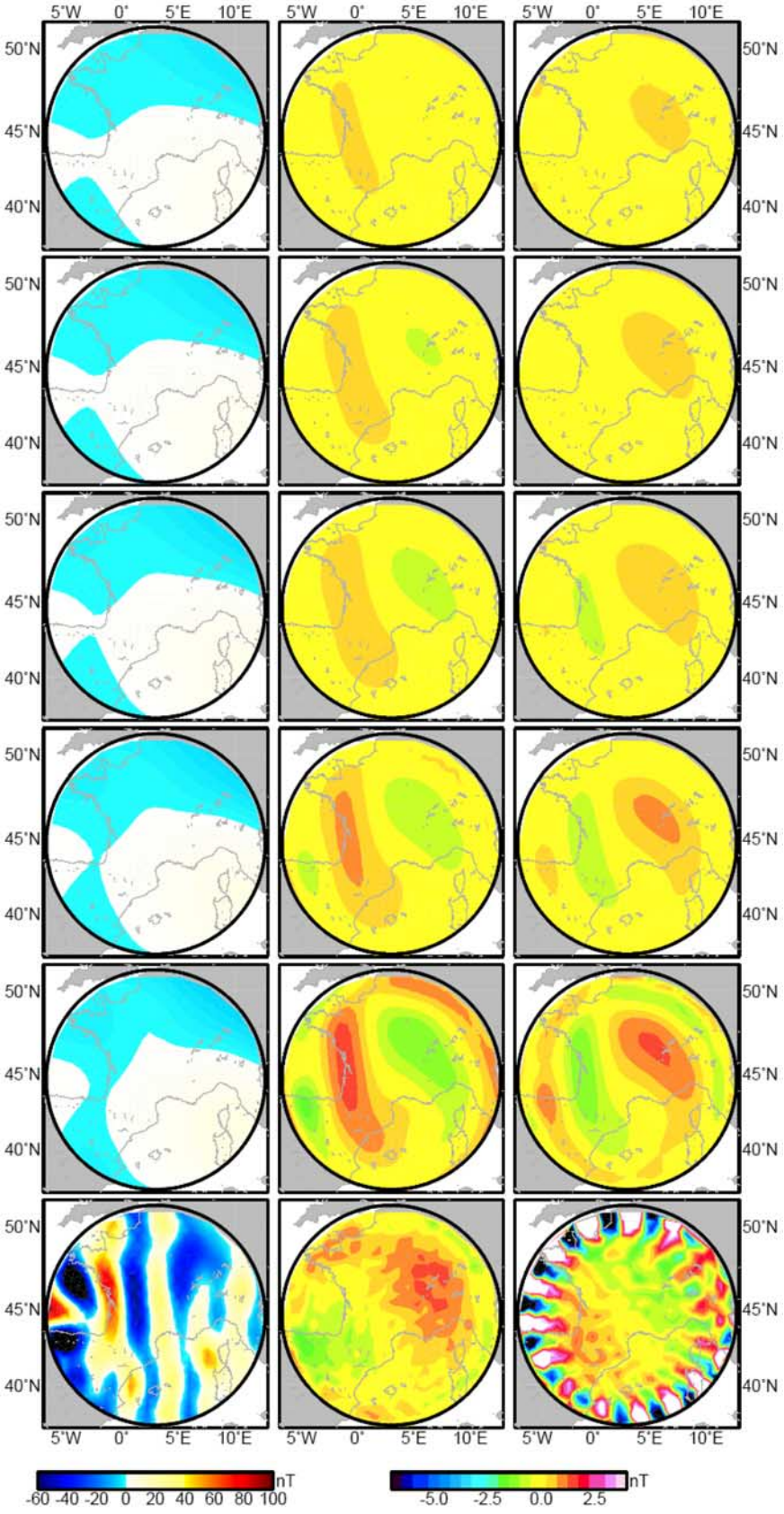


Figure 20. Same legend as in Figure 18 for Z.

SCHA is a physically well founded technique giving rise to robust parameter estimation, while SCHA parameter values depend on the maximum series expansion index. All the conclusions above have been obtained on synthetic vector data and discussed by looking at residual maps. They have to be interpreted in the light of the particular characteristics of the synthetic data set used, particularly the wavelengths contained in the input data and the aperture of the considered cap.

Acknowledgments

[40] We would like to acknowledge the thorough review of M. Korte and P. Kotzé. All figures in the manuscript were produced with GMT [*Wessel and Smith*, 1991]. For IPGP, this is contribution 2370.

References

De Santis, A., C. Falcone, and J. M. Torta (1996), Simple additional constraints on regional models of the geomagnetic secular variation field, *Phys. Earth Planet. Inter.*, *97*, 15–21.

De Santis, A., J. M. Torta, and F. J. Lowes (1999), Spherical cap harmonics revisited and their relationship to ordinary spherical harmonics, *Phys. Chem. Earth A*, *24*(11–12), 935–941.

Friis-Christensen, E., H. Lühr, and G. Hulot (2006), Swarm: A constellation to study the Earth's magnetic field, *Earth Planets Space*, *58*, 351–358.

Gaya-Piqué, L. R., J. J. Curto, J. M. Torta, and A. Chulliat (2008), Equivalent ionospheric currents for the 5 December 2006 solar flare effect determined from spherical cap harmonic analysis, *J. Geophys. Res.*, doi:10.1029/2007JA012934, in press.

Haines, G. V. (1985), Spherical cap harmonic analysis, *J. Geophys. Res.*, *90*(B3), 2583–2591.

Haines, G. V. (1988), Computer programs for spherical cap harmonic analysis of potential and general fields, *Comput. Geosci.*, *14*(4), 413–447.

Haines, G. V., and J. M. Torta (1994), Determination of equivalent current sources from spherical cap harmonic models of geomagnetic field variations, *Geophys. J. Int.*, *118*, 499–514.

Hamoudi, M., E. Thébault, V. Lesur, and M. Mandea (2007), GeoForschungsZentrum Anomaly Magnetic Map (GAMMA): A candidate model for the World Digital Magnetic Anomaly Map, *Geochem. Geophys. Geosyst.*, *8*, Q06023, doi:10.1029/2007GC001638.

Hitchman, A., and A. Lewis (2007), Observatory contributions to regional reference field models in the satellite ERA—The Australian experience, paper presented at XXIV General Assembly, Int. Union of Geod. and Geophys., Perugia, Italy, 2–13 July.

Korte, M., and V. Haak (2000), Modelling European magnetic repeat station and survey data by SCHA in search of time-varying anomalies, *Phys. Earth Planet. Inter.*, *122*, 205–220.

Korte, M., and R. Holme (2003), Regularization of spherical cap harmonics, *Geophys. J. Int.*, *153*, 253–262.

Korhonen, J. V., et al. (2007), Magnetic anomaly map of the world, scale 1:50,000,000, Comm. for the Geol. Map of the World, Paris.

Kotzé, P. B., M. Mandea, and M. Korte (2007), Geomagnetic field models for Southern Africa during 2005–2006, paper presented at XXIV General Assembly, Int. Union of Geod. and Geophys., Perugia, Italy, 2–13 July.

Maus, S., M. Rother, C. Stolle, W. Mai, S. Choi, H. Lühr, D. Cooke, and C. Roth (2006), Third generation of the Potsdam Magnetic Model of the Earth (POMME), *Geochem. Geophys. Geosyst.*, *7*, Q07008, doi:10.1029/2006GC001269.

Olsen, N., R. Haagmans, T. J. Sabaka, A. Kuvshinov, S. Maus, M. E. Purucker, M. Rother, V. Lesur, and M. Mandea (2006), The Swarm end-to-end mission simulator study: Separation of the various contributions to Earth's magnetic field using synthetic data, *Earth Planets Space*, *58*, 359–370.

Olsen, N., T. J. Sabaka, and L. R. Gaya-Piqué (2007), Study of an improved comprehensive magnetic field inversion analysis for Swarm, *DNSC Sci. Rep., 1/2007*, 110 pp., Dan. Natl. Space Cent., Copenhagen, Denmark.

Ravat, D., Whaler, M. Pilkington, T. Sabaka, and M. Purucker (2002), Compatibility of high-altitude aeromagnetic and satellite-altitude magnetic anomalies over Canada, *Geophysics*, *67*, 546–554.

Thébault, E. (2003), Modélisation régionale du champ magnétique terrestre, Ph.D. thesis, 268 pp., Univ. Louis Pasteur, Strasbourg, France, 17 Oct.

Thébault, E. (2008), A proposal for regional modelling at the Earth's surface, R-SCHA2D, *Geophys. J. Int.*, doi:10.1111/j.1365-246X.2008.03823.x, in press.

Thébault, E., J. J. Schott, M. Mandea, and J. P. Hoffbeck (2004), A new proposal for spherical cap harmonic modelling, *Geophys. J. Int.*, *159*, 83–103, doi:10.1111/j.1365-246X.2004.02361.x.

Thébault, E., J. J. Schott, and M. Mandea (2006a), Revised spherical cap harmonic analysis (R-SCHA): Validation and properties, *J. Geophys. Res.*, *111*, B01102, doi:10.1029/2005JB003836.

Thébault, E., M. Mandea, and J. J. Schott (2006b), Modeling the lithospheric magnetic field over France by means of revised spherical cap harmonic analysis (R-SCHA), *J. Geophys. Res.*, *111*, B05102, doi:10.1029/2005JB004110.

Torta, J. M., and A. De Santis (1996), On the derivation of the Earth's conductivity structure by means of spherical cap harmonic analysis, *Geophys. J. Int.*, *127*, 441–451.

Torta, J. M., A. García, J. J. Curto, and A. De Santis (1992), New representation of geomagnetic secular variation over restricted regions by means of spherical cap harmonic analysis: application to the case of Spain, *Phys. Earth. Planet. Inter.*, *74*, 209–217.

Torta, J. M., J. J. Curto, and P. Bencze (1997), Behavior of the quiet day ionospheric current system in the European region, *J. Geophys. Res.*, *102*(A2), 2483–2494.

Torta, J. M., L. R. Gaya-Piqué, and A. De Santis (2006), Spherical cap harmonic analysis of the geomagnetic field with application for aeronautical mapping, in *Geomagnetics for Aeronautical Safety: A Case Study in and Around the Balkans*, edited by J. L. Rasson and T. Delipetrov, pp. 291–307, Springer, Dordrecht, Netherlands.

Wessel, P., and W. H. F. Smith (1991), Free software helps map and display data, *Eos Trans. AGU*, *72*, 441.